ARTICLE

Synchronized Quartz Crystal Microbalance and Nanoplasmonic Sensing of Biomolecular Recognition Reactions

Andreas B. Dahlin,[†] Peter Jönsson, Magnus P. Jonsson, Emanuel Schmid,[‡] Ye Zhou,[§] and Fredrik Höök[†,*]

Division of Solid State Physics, Department of Physics, Lund University, Lund, Sweden. [†]Current address: Division of Biological Physics, Department of Applied Physics, Chalmers University of Technology, Gothenburg, Sweden. [‡]Current address: Swiss Federal Laboratories for Materials Testing and Research (EMPA), Dübendorf, Switzerland. [§]Current address: Institute of Physics, Chinese Academy of Sciences, Beijing, China.

ABSTRACT We present a method providing synchronized measurements using the two techniques: quartz crystal microbalance with dissipation (QCM-D) monitoring and localized surface plasmon resonance (LSPR). This was achieved by letting a thin gold film perforated with short-ranged ordered plasmon-active nanoholes act as one of the electrodes of a QCM-D crystal. This enabled transmission-mode optical spectroscopy to be used to temporally resolve colorimetric changes of the LSPR active substrate induced upon biomolecular binding events. The LSPR response could thus be compared with simultaneously obtained changes in resonance frequency, Δf, and energy dissipation, ΔD, of the QCM-D device. Since the LSPR technique is preferentially sensitive to changes within the voids of the nanoholes, while the QCM-D technique is preferentially sensitive to reactions on the planar region between the holes, a surface chemistry providing the same binding kinetics on both gold and silica was used. This was achieved by coating the substrate with poly(L-lysine)-graft-poly(ethylene glycol) (PLL-*g*-PEG), which was shown to bind in the same manner on silica and gold modified with a carboxyl-terminated thiol. In this way, the combined setup provided new information about structural changes upon PLL-*g*-PEG adsorption. We also demonstrate subsequent binding of NeutrAvidin and an immunoreaction utilizing biotin-modified IgG. The combined information from the synchronized measurements was also used in a new way to estimate the sensing volume of the LSPR sensor.

KEYWORDS: biosensor · quartz crystal microbalance · localized surface plasmon resonance · immunoreaction · apertures · ethyleneglycol · avidin

In 1959, Sauerbrey demonstrated that, when a film is adsorbed on a quartz crystal microbalance (QCM) surface, there is a shift in resonance frequency (f) proportional to the added mass. This assumption is valid as long as the mass is small compared to the weight of the crystal, rigidly attached and evenly distributed over the active area of the crystal.[1] The sensing principle of a QCM device is based on the variation in the electromechanical response of a shear-oscillating piezoelectric quartz crystal, caused by, for example, binding events or structural transformations in the adsorbed film. The technique was originally utilized almost exclusively in vacuum or gas phase,[2] but the work in 1980 by Nomura and co-workers demonstrated that the QCM could also be used for liquid-phase applications.[3] This paved the way for numerous new applications for the technique, especially in electrochemistry and biotechnology, in the latter case primarily for various biosensor applications (see the review by Andreas Janshoff[4]).

It was soon realized that, in liquid-phase studies, the mass obtained by QCM measurements does not correspond to the mass of adsorbed macromolecular entities since there is also a contribution from water dynamically coupled to the film.[5] In addition, when the damping in nonrigid adsorbed films due to frictional (viscous) losses becomes sufficiently large, the simple linear relation between Δf and adsorbed mass is no longer valid.[6] This leads to two new requirements to improve the usefulness of QCM as a quantitative sensor technique. The first is technical solutions that in addition to changes in resonance frequency provide information about changes in energy dissipation, ΔD, of the oscillating system. The second requirement is suitable theories to make full use of this new information. Information about changes in D can be obtained *via* either impedance spectroscopy[7] or, alternatively, as done in previous work by our group, by recording the oscillation decay of the freely oscillating crystal after rapid excitation at resonance.[8] In the latter case, the decay time constant is inversely proportional to the energy dissipation, D. Theoretically, the expressions for Δf and ΔD for a QCM crystal placed in an infinite viscous fluid are[9]

*Address correspondence to fredrik.hook@chalmers.se.

Received for review April 30, 2008 and accepted August 28, 2008.

Published online September 19, 2008.
10.1021/nn800254h CCC: $40.75

$$\Delta f = -\frac{1}{2\pi t_q \rho_q}\sqrt{\frac{\omega \rho_f \eta_f}{2}} \quad (1)$$

$$\Delta D = \frac{1}{t_q \rho_q}\sqrt{\frac{2\rho_f \eta_f}{\omega}} \quad (2)$$

where t_q is the thickness of the quartz crystal, ρ_q the density of quartz, ρ_f the density of the fluid, η_f the viscosity of the fluid, and ω the angular frequency of the oscillation. However, most biological films cannot be described by eqs 1 and 2, as they are not only viscous but also elastic and since they cannot be treated as infinite. A pioneering step in describing these kinds of situations was taken in the mid-1990s by Johannsmann and co-workers, demonstrating a theoretical description capable of representing the QCM-D response for viscoelastic films probed in either air or liquids.[10] We[11] and others[7] have utilized the multiparameter information contained in *f* and *D* measurements with analogous viscoelastic representations, capable of providing information not only about coupled mass but also about changes in the viscoelastic components of adsorbed films.[5] However, these models only estimate the total coupled mass and still face the challenge of distinguishing the actual biomolecular mass from dynamically coupled solvent.[12]

In cases when the analyzed films are sufficiently rigid (low *D*), the linear relation between changes in frequency and coupled mass is a safe assumption even in the case with coupled solvent and thus comparisons between different systems analyzed with QCM alone (*i.e.*, without combined *f* and *D* measurements) is feasible. However, important information, in particular with respect to coupled solvent, is achieved by operating the QCM technique in parallel with complementary methods such as (i) optical techniques like ellipsometry,[5,13] optical waveguide lightmode spectroscopy,[6] or surface plasmon resonance;[14,15] (ii) scanning probe microscopy;[16,17] and (iii) techniques engaging external molecular labels such as fluorescence or radio labeling.[18] For the optical techniques listed above, the measured signal originates from the polarizability (refractive indices) of the (bio)macromolecules under the influence of an incident electric field that is often locally amplified in the sensing region. Due to the close to linear relation (d*n*/d*c*) that exists between changes in the (bio)macromolecule concentration and the effective refractive index, this measurement principle has become extremely popular for quantifications of the adsorbed molecular mass.[19] Still, with a multitechnique approach based on different signal transduction mechanisms, there is a potential to access more information about the investigated interactions, such as binding pathways, stoichiometric ratios, transition states, phase transitions, and structural changes.

With few exceptions,[12,20,21] previous combinations of different surface analytical tools have not attempted simultaneous recording of binding kinetics but comparisons of saturated responses only. Johannsmann and co-workers demonstrated how propagating surface plasmons could be excited on a QCM sensor crystal modified with an optical grating.[20] Recently, the QCM-D technique was also combined with optical reflectometry readout (Wang *et al.*, *Rev. Sci. Instrum.*, accepted). We demonstrate in this work how the sensing electrode of a QCM crystal can be made into a plasmonic nanostructure, thus enabling acquisition of simultaneous information of changes in local refractive index, mechanically coupled mass (*via* Δf), and changes in the damping (*via* ΔD) of a QCM crystal. This was achieved by modifying one of the QCM gold electrodes with plasmonic nanometric apertures, the optical properties of which depend strongly on the refractive index of the surrounding medium within tens of nanometers of the surface.[22] While the vast majority of nanoplasmonic-based sensors have utilized discrete nanoparticles,[23−25] our group has put focus on thin gold films with short-range ordered (randomly distributed on the long-range) nanoscale apertures.[22,26−29] In contrast to a substrate with isolated nanoparticles, a gold film with randomly distributed holes is electrically conductive while the plasmonic properties are similar. In addition, the high conductivity of such a substrate allows it to act as one of the working electrodes of a QCM sensor. By letting the backside electrode have a ring configuration, we show in this work how conventional transmission-mode optical spectroscopy of the temporal variation in extinction peak position (color) of the surface can be synchronized with Δf and ΔD measurements from the very same surface.

Guided by the QCM-D data, which through viscoelastic modeling provide a measure of the effective film thickness, a new way to estimate the sensing depth associated with the highly localized field surrounding the plasmonically active apertures is proposed. As a model system for these estimations, as well as to demonstrate the sensing capability of the sensor design, we investigated subsequent modification of the sensor substrate with (i) a 1:1 mixture of biotinylated and unmodified poly(L-lysine)-graft-poly(ethylene glycol) (PLL-*g*-PEG),[30−32] (ii) NeutrAvidin, (iii) biotin-modified immunoglobulin G (anti-IgG), and (iv) immunoglobulin G (IgG).[33]

RESULTS AND DISCUSSION

The shifts in resonance frequency and dissipation at the fundamental resonance and at odd harmonics were measured by operating the crystal as described previously,[34] with the exception that the modified crystal was mounted in a home-built flow cell enabling optical access for transmission-mode spectroscopy. Measurements of the optical spectrum of the LSPR-active

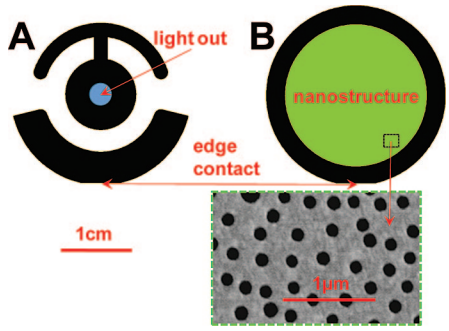

Figure 1. Illustration of the design of the back (A) and active (B) electrode in the synchronized QCM-D and LSPR setup. The ring on the active side is in contact with one of the electrodes on the backside by a thin metal layer on the edge of the crystal. The plasmonic nanostructure (green area) of the active electrode is compatible with transmission-mode extinction spectroscopy *via* the hole in the backside electrode (blue area). Also shown is a characteristic electron microscope image of the sensor surface.

electrode were enabled as described previously[27] by introducing a hole in the backside electrode (Figure 1).

The frequency spectrum in water from the LSPR-active crystals was compared to the corresponding spectrum from a standard 5 MHz QCM crystal (Figure 2). While the difference in resonance frequency is attributed to differences in the thickness of the quartz plate and the electrode, it is interesting to note that there was only a slight reduction in the quality factor, *Q*, for the modified crystal compared to the standard crystal, although additional smaller peaks besides the strong resonant peak are observed in the frequency spectrum of the modified crystal. However, despite the rather drastic changes in the electrode configuration, both the frequency and dissipation are considered similar to the values for a standard QCM crystal. It is also worthwhile to point out that the noise level, evaluated from measurements in aqueous solution, was roughly 0.4 Hz for the frequency and 0.04×10^{-6} for the dissipation at the third harmonic frequency, which is comparable with state of the art QCM instruments. Altogether this indicates that the modification of the electrode layout to make a LSPR-active surface has only a small influence on the basic behavior of the QCM crystals. The optical spectrum of the LSPR-active electrode showed a hole plasmon resonance at 565 ± 10 nm (Figure 2B) and was not influenced by operating the crystal in resonance.

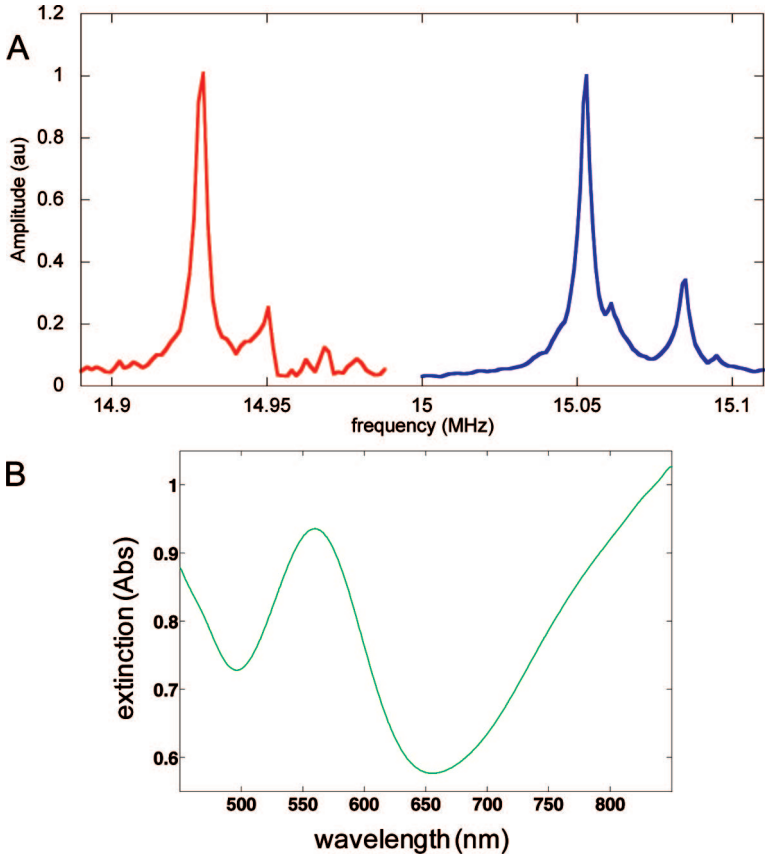

Figure 2. (A) Acoustic resonance shown as amplitude *versus* frequency spectrum around the first overtone (~15 MHz) for crystals with a continuous 200 nm gold electrode (red) and the ring-electrode configuration (blue), where the active electrode consists of a 55 ± 2 nm thick gold film perforated with randomly distributed ~110 ± 5 nm apertures. The shift in resonance frequency of the two crystals is attributed to differences in the mass of the electrodes. (B) Plasmonic resonance shown as extinction spectrum of the nanoholes. The resonance peak is superimposed on a background extinction from the nanostructure Au film.[29] All data were obtained with the sensing side of the crystal immersed in aqueous solution.

To test the sensitivity of the modified crystals, and whether they respond to a change in the surrounding medium as expected from theory (eqs 1 and 2), a modified crystal was exposed to increasing concentrations of glycerol in water. At the same time, the hole plasmon resonance peak position for the transmitted light through the LSPR-active sample was determined.[27] The results are shown in Figure 3, where the QCM-D data are acquired at the 3rd harmonic (15 MHz).

From Figure 3A, it is seen that both the frequency and dissipation shifts for the various glycerol concentrations are fairly well represented by eqs 1 and 2. The deviations from the theoretical values are essentially within the experimental error, although the dissipation shift may be considered slightly lower than expected. A possible interpretation of this result is that water entrapped in the nanoscale apertures couples to the crystal as a rigid mass and will therefore not contribute significantly to the damping of the crystal. This also means that, for the volume inside the apertures, a change in density of the solvent will alter the resonance frequency according to the Sauerbrey relation and not according to eqs 1 and 2. Still, with 55 nm deep holes and a hole coverage of ~10% of the surface area, a change from pure water to 35% glycerol in the void volume of the holes is expected to result in a decrease in frequency of less than 10 Hz, which is insignificant compared with the observed frequency shift of around 1 kHz. Thus, upon changes

in the properties of the bulk solution, a QCM crystal with a nanostructured electrode is expected to behave similarly to a standard QCM crystal in terms of both changes in f and in D. For otherwise identical, but approximately two times thinner metal electrodes, both Δf and ΔD were observed to be ~10% lower than for standard crystals (Jonsson *et al.*, *Anal. Chem.*, accepted), tentatively attributed to an influence from increasing glycerol concentrations on the bulk conductivity and, as a consequence, the effective conductivity of the electrode.[35] In agreement with previous results for nanoplasmonic sensors,[22,25−28] the resonance wavelength changes linearly with small increments in bulk refractive index. The sensitivity, corresponding to the slope of the linear fit, was typically ~50 nm/RI unit but varied between 40 and 60 nm for different samples. This variation is attributed to variations in the fabrication process.

The nanostructure composed of two different materials on the sensor surface (SiO_2 in the bottom of the holes surrounded by Au) has important implications on the use of the combined QCM-D and LSPR sensor to probe interfacial binding reactions. In contrast to QCM, which primarily will be sensitive to binding on the planar regions of the substrate since this constitutes most of the area, aperture-based nanoplasmonic sensing has the sensitivity highly focused to the void of the holes.[22,26,29] Thus, binding to the SiO_2 regions in the bottom of the holes will contribute significantly to the observed LSPR signal. As a consequence, different surface modifications of the hole bottom (SiO_2) and the Au regions may complicate a comparison of the QCM-D and the LSPR responses. To make a proper comparison between LSPR and QCM-D data, it is thus critical to ensure that that the binding is identical on SiO_2 and Au. To meet this demand, Au was modified with a short carboxyl-terminated alkanethiol, which renders also the Au region negatively charged. Upon exposure of SiO_2 and Au-coated standard QCM-D crystals to a 1:1 molar mixture of PLL-*g*-PEG:PLL-*g*-PEGbiotin, which binds by electrostatic interaction,[31] essentially identical binding reactions were observed (Figure 4). Furthermore, subsequent addition of NeutrAvidin displayed the same binding behavior on the two materials. As control experiment, NeutrAvidin was added together with free biotin in solution, which resulted in no detectable binding to any of the surfaces, verifying the inert background provided by the PEG chains (not shown).

Figure 5 shows changes in frequency, Δf, and peak position, $\Delta\lambda_{peak}$, *versus* time upon addition of the same mixtures as in Figure 4, but using the combined QCM-D and LSPR sensor surface modified with thiols. Addition of the PLL-*g*-PEG:PLL-*g*-PEGbiotin mixture (step 1 in Figure 5A) results in a rapid decease in frequency and a red shift in peak position saturating at around -35 ± 2 Hz and 0.5 ± 0.01 nm, respectively. Despite a hole coverage of 12%, and a corresponding increase in total area of ~20% from the hole walls, the QCM response

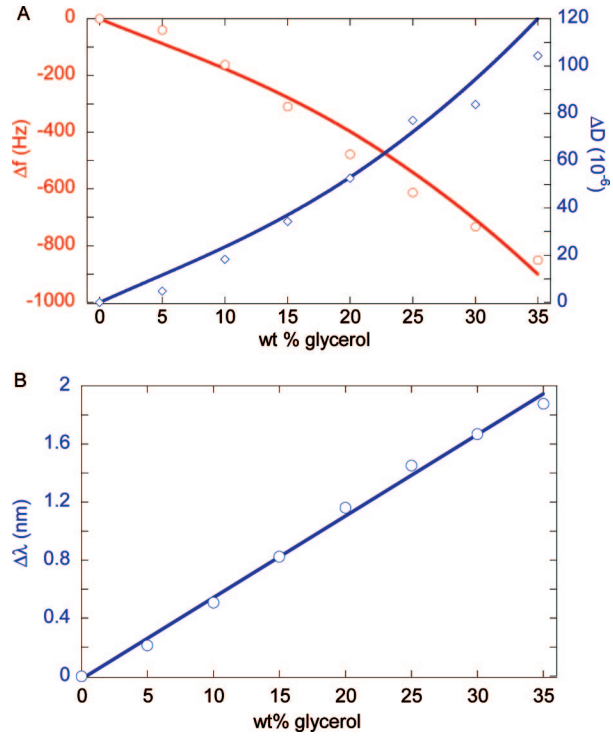

Figure 3. (A) Changes in frequency, Δf (red circles), and dissipation, ΔD (blue circles), *versus* increasing concentrations of glycerol in water relative to pure water. The solid lines are theoretical values from eqs 2 and 3 at the 3rd harmonic (15 MHz), where data on the density and the viscosity at 25 °C were obtained from the specifications provided by The Dow Chemical Company (http://www.dow.com/glycerine/resources/physicalprop.htm). The density of quartz used was set to 2650 kg/m^3 and the shear wave velocity to 3340m/s.[40] (B) Changes in peak position, $\Delta\lambda_{peak}$ (circles), *versus* refractive index upon increasing glycerol concentration as in previous work.[22,26−28] The absolute peak position of the sample in pure water is around 565 nm. The solid line is a linear fit to the data points yielding a typical sensitivity of ~50 nm/RI unit (varying between 40 and 60 nm for different samples).

is in good agreement with the results on homogeneous SiO_2 crystals and on carboxyl-terminated homogeneous Au crystals (see Figure 4). This is consistent with the fact that the QCM technique senses the water in the voids of the holes as a rigid mass. As a conse-

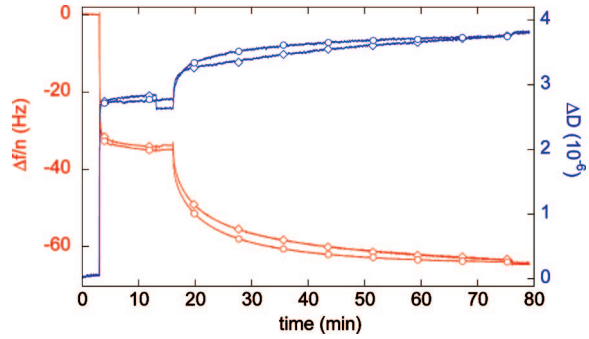

Figure 4. QCM-D data upon exposure (t ~ 3 min) to a 1:1 mixture of PLL-*g*-PEG and PLL-*g*-PEGbiotin followed by addition of NeutrAvidin (t ~ 16 min). The shifts in f (red) and D (blue) are seen to be nearly identical on Au (circles) and SiO_2 (diamonds) surfaces, both incubated with carboxylic acid thiols. The flow cell was rinsed at t = 13 min and t = 76 min.

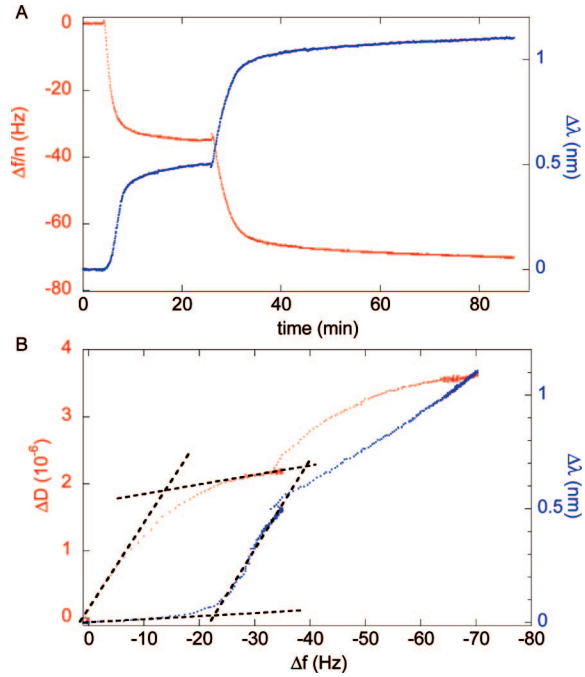

Figure 5. (A) Changes in frequency (red) and peak position (blue) *versus* time upon exchange of a buffer solution at $t = 4$ min to a 1:1 mixture of PLL-*g*-PEG and PLL-*g*-PEGbiotin (0.1 mg/mL) followed by subsequent additions of NeutrAvidin (0.3 μM) at $t = 27$ min. (B) ΔD and $\Delta\lambda_{peak}$ *versus* Δf for the sequence of additions shown in Figure 3.

quence, the fraction of the PLL-*g*-PEG that replaces coupled water within the hole will, due to the small difference (~30%) in density between PLL-*g*-PEG and water, not contribute significantly to changes in the frequency. However, water coupled to the adsorbed molecules at the upper edges of the nanoholes will be sensed as an additional mass. It is reasonable to assume that these effects balance each other, thus explaining why essentially identical QCM responses were observed for the nanostructured and planar surfaces.

At first sight, the kinetics of the LSPR and QCM responses appear very similar (Figure 5A). However, a detailed inspection of the data reveals interesting differences that would not have been possible to resolve if the QCM and LSPR responses were not synchronized. In particular, by plotting the peak position shift, $\Delta\lambda_{peak}$, *versus* Δf, an essentially linear slope is observed upon NeutrAvidin binding, while in the case of PLL-*g*-PEG binding, at least two different slopes are clearly distinguishable. Strikingly, at low coverage ($\Delta f < -20$ Hz and $\Delta\lambda_{peak} < 0.05$ nm), the slope is a factor of almost 10 lower than at high coverage (see the dashed black lines in Figure 5B). To interpret this observation, it is important to recall that the LSPR response is proportional to the change in interfacial refractive index.[36] Since there is also a linear relation between the increment in refractive index and concentration of most biomolecules and polymers, the LSPR response is proportional to the number of bound entities as long as the binding occurs without significant structural changes or multilayer formation and there is no preferential adsorption at LSPR-sensitive regions. In contrast, the QCM technique senses in addition to the mass of adsorbed entities also hydrodynamically coupled solvent. Since the amount of coupled solvent may vary with coverage,[12] the interpretation of binding kinetics from QCM data is often complicated. Note, however, that there is an essentially linear $\Delta\lambda_{peak}$ *versus* Δf slope upon binding of NeutrAvidin, which signals that the amount of coupled solvent does not change with coverage in this case. The much lower value of the initial slope at low PLL-*g*-PEG coverage suggests an initial formation of a film with a significant amount of coupled solvent, whereas there is a structural change at a coverage of about 10% ($\Delta\lambda_{peak} \sim 0.05$ nm), after which the amount of coupled solvent is significantly lower.

The much larger contrast observed in the transition of the $\Delta\lambda_{peak}$ *versus* Δf slope than of the ΔD *versus* Δf slope can also be explained by structural changes of adsorbed PLL-*g*-PEG, such as transformations from an extended to a more confined state, and thus into a region with stronger electromagnetic field. Such structural changes are expected to be visible as an acceleration in the LSPR response, as we have shown for the case of bilayer formation from lipid vesicles,[28] and a weak acceleration in $\Delta\lambda_{peak}$ is in fact visible in the kinetics data just after PLL-*g*-PEG addition (Figure 5). An alternative, and probably more likely, interpretation is that differences in binding behavior of PLL-*g*-PEG at regions of high and low LSPR sensitivity contribute to the observed data. One possible scenario is that binding of PLL-*g*-PEG initially occurs preferentially on the planar Au film, where the LSPR and QCM sensitivities are low and high, respectively, while the later phase primarily corresponds to binding in the voids of the holes, where the sensitivities are reversed (see above). This could potentially be explained by the relatively deep (55 nm) holes acting as a steric hindrance that reduces the probability of adsorption to the bottom of the holes.[26] In solution, a single PLL-*g*-PEG molecule is over 60 nm in size,[30] which is comparable to the hole diameter of 110 nm. This type of effect on the binding kinetics, potentially related to the nanostructure on the surface, will be investigated using planar surfaces where QCM-D is combined with reflectometry (Wang *et al.*, *Rev. Sci. Instrum.*, accepted) or conventional SPR.[12]

Theories capable of translating peak-position changes of these types of LSPR-active sensing templates into absolute numbers of adsorbed molecules are yet to be developed, which means that it is not straightforward to quantify the adsorbed molecular mass from the LSPR response. However, as shown in a parallel work (Jonsson *et al.*, *Anal. Chem.*, accepted), combined QCM-D and LSPR data can indeed be used to aid a quantitative interpretation of LSPR data. Here we instead use previously published data[33] from conventional SPR, with the same surface modification of Au

TABLE 1. Summary of Data Obtained Using SPR, QCM-D, and LSPR

	SPR		QCM-D			LSPR
layers	response (RU)	Δm_{SPR}[a] (ng/cm^2)	Δf (Hz)	Δm[c] (ng/cm^2)	d[c] (nm)	$\Delta\lambda_{peak}$ (nm)
PLL-*g*-PEG	2130	166[b]	−34.7	655	6.9	0.5
NeutrAvidin	2370	158	−35.0	685	7.2	0.6

[a]The SPR mass was estimated using the well-established relation between changes in resonance units (ΔRU) and mass uptake (1RU = 0.1 ng/cm^2) divided by 1.5 to take into account the fact that binding occurred on a planar surface, rather than an extended dextran hydrogel.[41] [b]This value was estimated by correcting the mass uptake conversion of SPR data for the differences in refractive index increment between PLL-*g*-PEG and proteins. The values of the refractive index increment were $dn/dc_{biotin\text{-}PLL\text{-}PEG}$ = 0.158 cm^3/g and $dn/dc_{NeutrAvidin}$ = 0.185 cm^3/g as in previous work.[33] [c]These values are obtained from a Voigt-based analysis of the QCM-D data.

as described above to get the adsorbed molecular mass (see Table 1 for a summary of the results). Together with the LSPR data and a Voigt-based analysis[5] of the QCM-D data to get the thickness of the film, the mass uptake from the SPR measurements yields sufficient information to estimate the sensing depth of the LSPR substrate as shown below.

Starting from the bulk experiment (Figure 3), it is clear that the LSPR peak shift is linearly related to the surrounding refractive index for homogeneous changes in the whole liquid volume. This is in agreement with previous reports on LSPR sensors based on both nanoholes[22,26,27] and nanoparticles,[25] even if the linear relation is not always true for substantial changes in refractive index.[28] We can thus, as a good approximation, relate $\Delta\lambda_{peak}$ to Δn_{eff} as

$$\Delta\lambda_{peak} = k\Delta n_{eff} \tag{3}$$

where k is the slope of the graph in Figure 3 (~50 nm/RIU) and n_{eff} is the effective surrounding refractive index, defined as the integral of the refractive index in the entire liquid volume with a weighting function to compensate for the spatial inhomogeneity of the sensitivity. In conventional SPR, it has been shown that the square of the field distribution $E(x,y,z)$ can be used as weight to calculate n_{eff}.[19] Using the same reasoning for LSPR structures, n_{eff} can be defined as

$$\Delta n_{eff} = \frac{\int\int\int_V \Delta n(x,y,z)E^2(x,y,z)\mathrm{d}x\mathrm{d}y\mathrm{d}z}{\int\int\int_V E^2(x,y,z)\mathrm{d}x\mathrm{d}y\mathrm{d}z} \tag{4}$$

where V denotes the entire (liquid) volume within which a change in n (relative to the RI of the buffer) can occur. For mathematical reasons, E is set to zero outside the liquid volume where no changes in refractive index occur although the plasmon field does extend also into other regions, in this case the quartz substrate. The denominator integral in eq 4 is introduced for normalization, so that $\Delta n_{eff} = \Delta n$ for changes in bulk RI.

It is reasonable to assume a linear relation between biomolecular concentration and changes in $n(x,y,z)$ within a thin film;[37] that is, RI changes are assumed to be homogeneous within the volume of the film and zero outside that volume. For such a volume V_i, we can define a *sensitivity fraction* α_i associated with the volume according to

$$\alpha_i = \frac{\int\int\int_{V_i} E^2(x,y,z)\mathrm{d}x\mathrm{d}y\mathrm{d}z}{\int\int\int_V E^2(x,y,z)\mathrm{d}x\mathrm{d}y\mathrm{d}z} \tag{5}$$

The sensitivity fraction thus represents how much of the total sensitivity k that is associated with a certain liquid volume V_i. For changes in RI that occur homogenously inside V_i, λ_{peak} responds with a sensitivity of $\alpha_i k$. A change in RI within a biomolecular layer i can furthermore be expressed as

$$\Delta n_i = \frac{\Gamma_i[dn/dc]_i}{d_i} \tag{6}$$

where d_i is the effective thickness of the layer, dn/dc_i is the refractive index dependence on the concentration, and Γ_i is the surface coverage of molecules.

Finally, by using eqs 4−6, eq 3 can be rewritten to express the peak shift as a sum of changes in n within different volumes, multiplied with their respective sensitivity fraction. This is under the assumption that local changes in refractive index do not affect the field distribution. The peak shift can then be written as

$$\Delta\lambda_{peak} = k\sum_i \alpha_i \frac{\Gamma_i[dn/dc]_i}{d_i} \tag{7}$$

Equation 7 can then be applied to determine the fraction of the total sensitivity k associated with the first two molecular layers by help of the QCM-D data. As shown in a previous work,[33] NeutrAvidin binds within the PLL-PEG film and causes a swelling of the adsorbed film. This is in agreement with the observed increase in thickness by 7 nm, which is larger than the diameter of the protein (~5 nm). The film composed of PLL-PEG and NeutrAvidin is thus treated as one homogeneous layer, with a total mass of Γ = 324 ng/cm^2 (Table 1). Since the total adsorbed mass of PLL-PEG and NeutrAvidin is similar, it is reasonable to use an average dn/dc value of 0.171 cm^3/g.[33] From a Voigt analysis,[5] the thickness, d, of the total layer was determined to 14 nm. Using the LSPR data, $\Delta\lambda_{peak}$ = 1.1 nm and k = 50 nm/RI unit, α becomes 0.56. Thus, approximately 56% of the sensitivity is localized within 14 nm of the surface. The primary error in the value of 56% is most likely the assumption that the PLL-PEG/NeutrAvidin layer is homogeneous, while in reality the NeutrAvidin molecules are probably on average further from the surface and exposed to a lower field strength than the PLL-

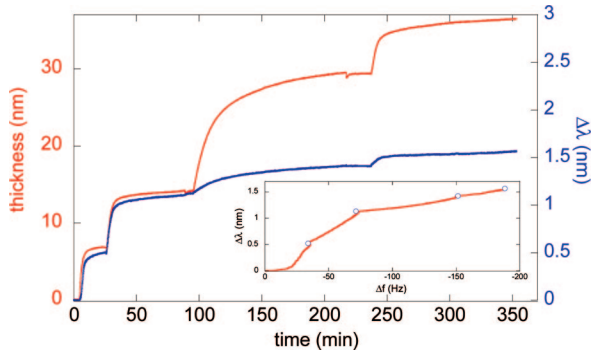

Figure 6. Changes in effective thickness (obtained *via* a Voigt-based modeling of the QCM-D data) and $\Delta\lambda_{peak}$ *versus* time upon exchange of a buffer solution at $t = 4$ min to a 1:1 mixture of PLL-*g*-PEG and PLL-*g*-PEGbiotin followed by subsequent additions of NeutrAvidin (these steps are identical to those in Figure 5A) followed by addition of biotin-IgG at $t = 96$ min and anti-IgG at $t = 238$ min. Inset: $\Delta\lambda_{peak}$ *versus* Δf for the same sequence of additions.

PEG. Still, the d*n*/d*c* values for these molecules differ by only ~10%. It should also be noted that the thiol modification of Au means that the sensing volume included in this calculation extends a little longer than 14 nm from the Au regions. The bulk refractive index sensitivity *k* depends strongly on the nanostructure dimensions[22,26,27] but is highly reproducible for a given sample. Finally, the 56% value is in agreement with parallel work (Jonsson *et al.*, *Anal. Chem.*, accepted) and with our previous study of supported lipid bilayer formation on silica-encapsulated LSPR-active nanoholes in gold films[28] and numerical simulations of similar nanoholes.[38]

The existence of a relatively extended LSPR sensing depth was verified by subsequently exposing the NeutrAvidin-coated PLL-*g*-PEG-modified QCM-D/LSPR surface to anti-IgG and IgG. Figure 6 shows a comparison of the temporal variation in film thickness obtained from a Voigt-based modeling of the QCM-D data and the temporal variation in $\Delta\lambda_{peak}$ upon these injections.

Indeed, the formation of a multilayer film with a thickness approaching 40 nm can still be probed using the LSPR template, but the reduction in sensitivity is clearly seen. Also note the almost linear relation between $\Delta\lambda_{peak}$ and Δf upon binding of IgG and anti-IgG, signals that the amount of coupled solvent does not vary significantly with coverage for these cases. This means, in turn, that the QCM-D data can be used to extract proper information about binding kinetics, which is not the case when there are significant structural changes involved, as in the case of PLL-*g*-PEG binding, indicated by the nonlinear relation between $\Delta\lambda_{peak}$ and Δf and between ΔD and Δf (see Figure 5 and the inset in Figure 6).

In conclusion, the information contained in multiparameter measurements of the type presented in this work illustrates how the combination of the sensor principles turns an apparent limitation with the QCM-D technique into an advantage and, *vice versa*, how the interpretation of LSPR data is supported by the information contained in QCM-D measurements. We believe this combined technique will prove a valuable tool for studying biomolecules on surfaces due to the fundamental differences between the QCM-D and LSPR techniques and the increased amount of information gained.

MATERIALS AND METHODS

Sensor Fabrication. Combined QCM-D/LSPR samples were fabricated from ~300 μm thick blank AT-cut quartz crystals (MaxTec Inc., USA) starting with cleaning in Piranha (3:1 by volume H_2SO_4(95%)/H_2O_2(30%); CAUTION: this mixture reacts spontaneously under generation of heat and is strongly corrosive and harmful to skin and eyes) followed by thorough rinsing with milli-Q water (Millipore, USA) and blow-drying with N_2. The backside electrode was defined by conventional UV lithography (MJB3 mask aligner, Karl Süss, Germany) followed by thermal evaporation of 5 nm Cr and 150 nm Au (AVAC, Sweden) (see Figure 1). A homogeneous distribution of nanoscale apertures in a thin Au electrode was created on the active side of the crystal by colloidal lithography[22,26−29,39] as follows: After an additional cleaning with Piranha, the surface was modified with a polyelectrolyte triple layer[39] which renders the surface positively charged. Negatively charged polystyrene colloids (110 nm, Interfacial Dynamics Corporation, USA) suspended in water were then self-assembled into a saturated monolayer on the surface; 1 nm Cr and 54 nm Au were deposited by thermal evaporation, and the apertures were finally realized by lift-off of the polystyrene colloids using tape, leaving 110 nm apertures with a characteristic short-range order and average coverage of 12 holes/μm^2. Before further use, the crystals were cleaned in acetone, isopropanol, and milli-Q water and dried with N_2. To improve electrical contact, a ring was fabricated on the nanostructured active side of the crystal close to the edge using the same procedure as for the backside electrode (see Figure 1). Also, a small stripe of 5 nm Cr and 150 nm Au was deposited on the 300 μm edge of the crystal, allowing the front electrode to be contacted from the back side of the crystal. The samples were then cleaned with RCA1 (5:1:1 by volume milli-Q water/NH_3 (25%)/H_2O_2 (30%); CAUTION: this mixture is corrosive and harmful to the eyes) at ~70 °C for 15 min followed by thorough rinsing with milli-Q water and drying with N_2. The quality of the nanostructures was confirmed using scanning electron microscopy (JEOL JSM6400F).

QCM-D and LSPR Measurement Setup. The combined setup for QCM-D and LSPR measurements on 1 in. crystals was made in house. The fluid was in all experiments introduced into the flow cell by gravity, through a metal beaker situated on top of the cell. The samples were mounted between two O-rings to relieve stress and electrically connected from the back side of the crystal by two spring-loaded contact pins. Two plastic plugs, consisting of a collimating lens and contact pins, provided optical and electrical connection to the sample through the measurement cell. A thermoelectric module, controlled by a temperature controller (MPT-5000 Wavelength Electronics, USA), was mounted on the side of the cell and stabilized the temperature to eliminate thermal drift. The extinction spectrum of the nanoholes was acquired by collecting light that was transmitted through the nanostructure (front electrode) and the hole in the backside electrode. Light from a tungsten−halogen lamp (OceanOptics HL-2000) was guided *via* an optical fiber and a collimation lens to the sample in the measurement cell. The spectrum of the transmitted light was measured by a spectrometer (BTC611E, B&WTek, USA). Spectral data were acquired with a frame rate of

0.5 Hz and continuously analyzed in MatLab (Mathworks Inc., USA) as described in previous work from our group[27] to yield the peak position λ_{peak} (corresponding to the wavelength at maximum extinction of light) with a resolution of around 10^{-3} nm. The setup used for QCM measurements was based on a QCM-D setup introduced by Rodahl and Kasemo.[8] In brief, a frequency generator (Agilent 33250A) controlled by GPIB was used to drive the oscillations, whereas a digital oscilloscope (Nicolet, model 490) monitored the oscillation decay. The resonance frequency and dissipation were calculated by a modified version of the commercial program Q-Soft (Q-sense, Sweden) for each overtone. All measurements were made at 25 °C. Solution exchange was rapid (<5 s), and kinetics data represent binding from stagnant bulk.

Surface Modification and Biomolecular Sensing. Prior to each measurement, samples were cleaned with RCA1, incubated in a solution containing 1 mM $HS-(CH_2)_{15}-COOH$ (kindly provided by the Dept. of Physics and Measurement Technology, Linköping University, Sweden) in ethanol (99.7%, Sigma) overnight, sonicated in ethanol, and dried with N_2. Biosensing experiments were done in HEPES buffer: 10 mM HEPES, 150 mM NaCl, pH adjusted to 7.4 with NaOH (chemicals from SigmaAldrich). PLL(20)-*g*[3.5]-PEG(2) (SurfaceSolutions, Switzerland) was stored in buffer at −6 °C. Antibody aniti-IgG and antigen IgG was provided by the Department of Immunotechnology at Lund University for these experiments.

Acknowledgment. This work was financially supported by the Swedish Research Council for Engineering Sciences, contract number 2005-3140, and the Ingvar grant from the Strategic Research Foundation.

REFERENCES AND NOTES

1. Sauerbrey, G. Verwendung von Schwingquarzen zur Wägung dünner Schichten und zur Mikrovägung. *Z. Phys.* **1959**, *155*, 206–222.
2. Lu, C.; Czanderna, A. W., *Applications of Piezoelectric Quartz Crystal Microbalances*; Elsevier: Amsterdam, 1984; Vol. 7.
3. Nomura, T.; Minemura, A. Behavior of a Piezoelectric Quartz Crystal in an Aqueous-Solution and the Application to the Determination of Minute Amount of Cyanide. *Nippon Kagaku Kaishi* **1980**, *10*, 1621–1625.
4. Janshoff, A.; Galla, H. J.; Steinem, C. Piezoelectric Mass-Sensing Devices as Biosensors—An Alternative to Optical Biosensors. *Angew. Chem., Int. Ed.* **2000**, *39*, 4004–4032.
5. Hook, F.; Kasemo, B.; Nylander, T.; Fant, C.; Sott, K.; Elwing, H. Variations in Coupled Water, Viscoelastic Properties, and Film Thickness of a Mefp-1 Protein Film during Adsorption and Cross- Linking: A Quartz Crystal Microbalance with Dissipation Monitoring, Ellipsometry, and Surface Plasmon Resonance Study. *Anal. Chem.* **2001**, *73*, 5796–5804.
6. Hook, F.; Vörös, J.; Rodahl, M.; Kurrat, R.; Böni, P.; Ramsden, J. J.; Textor, M.; Spencer, N. D.; Tengvall, P.; Gold, J.; et al. A Comparative Study of Protein Adsorption Kinetics and Saturation Uptake on Titanium Oxide Surfaces Using *In Situ* Ellipsometry, Optical Waveguide Lightmode Spectroscopy, and the Quartz Crystal Microbalance/Dissipation Techniques. *Colloids Surf., B* **2002**, *24*, 155–170.
7. Bandey, H. L.; Hillman, A. R.; Brown, M. J.; Martin, S. J. Viscoelastic Characterization of Electroactive Polymer Films at the Electrode/Solution Interface. *Faraday Discuss.* **1997**, *107*, 105–122.
8. Rodahl, M.; Höök, F.; Krozer, A.; Brzezinski, P.; Kasemo, B. Quartz Crystal Microbalance Set Up for Frequency and Q-Factor Measurements in Gaseous and Liquids Environments. *Rev. Sci. Instrum.* **1995**, *66*, 3924–3930.
9. Reed, C. E.; Kanazawa, K. K.; Kaufman, J. H. Physical Description of a Viscoelastically Loaded AT-Cut Quartz Resonator. *J. Appl. Phys.* **1990**, *68*, 1993–2001.
10. Domack, A.; Prucker, O.; Ruhe, J.; Johannsmann, D. Swelling of a Polymer Brush Probed with a Quartz Crystal Resonator. *Phys. Rev. E* **1997**, *56*, 680–689.
11. Rodahl, M.; Hook, F.; Fredriksson, C.; Keller, C. A.; Krozer, A.; Brzezinski, P.; Voinova, M.; Kasemo, B. Simultaneous Frequency and Dissipation Factor QCM Measurements of Biomolecular Adsorption and Cell Adhesion. *Faraday Discuss.* **1997**, *107*, 229–246.
12. Reimhult, E.; Larsson, C.; Kasemo, B.; Hook, F. Simultaneous SPR and QCM-D Measurements of Biomolecular Adsorption Events Involving Structural Transformations and Variations in Coupled Water. *Anal. Chem.* **2004**, *76*, 7211–7220.
13. Tjarnhage, T.; Puu, G. Liposome and Phospholipid Adsorption on a Platinum Surface Studied in a Flow Cell Designed for Simultaneous Quartz Crystal Microbalance and Ellipsometry Measurements. *Colloids Surf., B* **1996**, *8*, 39–50.
14. Caruso, F.; Furlong, D. N.; Kingshott, P. Characterization of Ferritin Adsorption onto Gold. *J. Colloid Interface Sci.* **1997**, *186*, 129–140.
15. Larsson, C.; Rodahl, M.; Hook, F. Characterization of DNA Immobilization and Subsequent Hybridization on a 2D Arrangement of Streptavidin on a Biotin-Modified Lipid Bilayer Supported on SiO_2. *Anal. Chem.* **2003**, *75*, 5080–5087.
16. Choi, K. H.; Friedt, J. M.; Frederix, F.; Campitelli, A.; Borghs, G. Simultaneous Atomic Force Microscope and Quartz Crystal Microbalance Measurements: Investigation of Human Plasma Fibrinogen Adsorption. *Appl. Phys. Lett.* **2002**, *81*, 1335–1337.
17. Richter, R. P.; Berat, R.; Brisson, A. R. Formation of Solid-Supported Lipid Bilayers: An Integrated View. *Langmuir* **2006**, *22*, 3497–3505.
18. Muratsugu, M.; Ohta, F.; Miya, Y.; Hosokawa, T.; Kurosawa, S.; Kamo, N.; Ikeda, H. Quartz Crystal Microbalance for the Detection of Microgram Quantities of Human Serum Albumin: Relationship between the Frequency Change and the Mass of Protein Adsorbed. *Anal. Chem.* **1993**, *65*, 2933–2937.
19. Jung, L. S.; Campbell, C. T.; Chinowsky, T. M.; Mar, M. N.; Yee, S. S. Quantitative Interpretation of the Response of Surface Plasmon Resonance Sensors to Adsorbed Films. *Langmuir* **1998**, *14*, 5636–5648.
20. Laschitsch, A.; Menges, B.; Johannsmann, D. Simultaneous Determination of Optical and Acoustic Thicknesses of Protein Layers Using Surface Plasmon Resonance Spectroscopy and Quartz Crystal Microweighing. *Appl. Phys. Lett.* **2000**, *77*, 2252–2254.
21. Su, X. D.; Wu, Y. J.; Robelek, R.; Knoll, W. Surface Plasmon Resonance Spectroscopy and Quartz Crystal Microbalance Study of Streptavidin Film Structure Effects on Biotinylated DNA Assembly and Target DNA Hybridization. *Langmuir* **2005**, *21*, 348–353.
22. Dahlin, A.; Zach, M.; Rindzevicius, T.; Kall, M.; Sutherland, D. S.; Hook, F. Localized Surface Plasmon Resonance Sensing of Lipid-Membrane-Mediated Biorecognition Events. *J. Am. Chem. Soc.* **2005**, *127*, 5043–5048.
23. Haes, A. J.; Van Duyne, R. P. A Nanoscale Optical Biosensor: Sensitivity and Selectivity of an Approach Based on the Localized Surface Plasmon Resonance Spectroscopy of Triangular Silver Nanoparticles. *J. Am. Chem. Soc.* **2002**, *124*, 10596–10604.
24. Kalyuzhny, G.; Vaskevich, A.; Schneeweiss, M. A.; Rubinstein, I. Transmission Surface-Plasmon Resonance (T-SPR) Measurements for Monitoring Adsorption on Ultrathin Gold Island Films. *Chem.—Eur. J.* **2002**, *8*, 3850–3857.
25. Nath, N.; Chilkoti, A. A Colorimetric Gold Nanoparticle Sensor to Interrogate Biomolecular Interactions in Real Time on a Surface. *Anal. Chem.* **2002**, *74*, 504–509.
26. Dahlin, A. B.; Jonsson, M. P.; Hook, F. Specific Self-Assembly of Single Lipid Vesicles in Nanoplasmonic Apertures in Gold. *Adv. Mater.* **2008**, *20*, 1436–1442.
27. Dahlin, A. B.; Tegenfeldt, J. O.; Hook, F. Improving the Instrumental Resolution of Sensors Based on Localized Surface Plasmon Resonance. *Anal. Chem.* **2006**, *78*, 4416–4423.

28. Jonsson, M. P.; Jonsson, P.; Dahlin, A. B.; Hook, F. Supported Lipid Bilayer Formation and Lipid-Membrane-Mediated Biorecognition Reactions Studied with a New Nanoplasmonic Sensor Template. *Nano Lett.* **2007**, *7*, 3462–3468.
29. Marie, R.; Dahlin, A. B.; Tegenfeldt, J. O.; Hook, F. A Generic Surface Modification Strategy for Sensing Applications Based on Au/SiO_2 Nanostructures. *Biointerphases* **2007**, *2*, 49–55.
30. Feuz, L.; Strunz, P.; Geue, T.; Textor, M.; Borisov, O. Conformation of Poly(L-lysine)-graft-poly(ethylene glycol) Molecular Brushes in Aqueous Solution Studied by Small-Angle Neutron Scattering. *Eur. Phys. J. E* **2007**, *23*, 237–245.
31. Huang, N. P.; Michel, R.; Voros, J.; Textor, M.; Hofer, R.; Rossi, A.; Elbert, D. L.; Hubbell, J. A.; Spencer, N. D. Poly(L-lysine)-g-poly(ethylene glycol) Layers on Metal Oxide Surfaces: Surface-Analytical Characterization and Resistance to Serum and Fibrinogen Adsorption. *Langmuir* **2001**, *17*, 489–498.
32. Huang, N. P.; Voros, J.; De Paul, S. M.; Textor, M.; Spencer, N. D. Biotin-Derivatized Poly(L-lysine)-g-poly(ethylene glycol): A Novel Polymeric Interface for Bioaffinity Sensing. *Langmuir* **2002**, *18*, 220–230.
33. Zhou, Y.; Xu, H.; Dahlin, A. B.; Gustafson, J.; Borrebaeck, C. A. K.; Wingren, C.; Liedberg, B.; Hook, F. Quantitative Interpretation of Gold Nanoparticle-Based Bioassays Designed for Detection of Immuno-Complex Formation. *Biointerphases* **2007**, *2*, 6–15.
34. Hook, F.; Rodahl, M.; Brzezinski, P.; Kasemo, B. Energy Dissipation Kinetics for Protein and Antibody-Antigen Adsorption Under Shear Oscillation on a Quartz Crystal Microbalance. *Langmuir* **1998**, *14*, 729–734.
35. Rodahl, M.; Höök, F.; Kasemo, B. QCM Operation In Liquids: An Explanation of Measured Variations in Frequency and Q Factor With Liquid Conductivity. *Anal. Chem.* **1996**, *68*, 2219–2227.
36. Willets, K. A.; Van Duyne, R. P. Localized Surface Plasmon Resonance Spectroscopy and Sensing. *Annu. Rev. Phys. Chem.* **2007**, *58*, 267–297.
37. Feijter, J. A. d.; Benjamins, J.; Veer, F. A. Ellipsometry as a Tool to Study the Adsorption Behavior of Synthetic and Biopolymers at the Air-Water Interface. *Biopolymers* **1978**, *17*, 1759–1772.
38. Rindzevicius, T.; Alaverdyan, Y.; Sepulveda, B.; Pakizeh, T.; Kall, M.; Hillenbrand, R.; Aizpurua, J.; de Abajo, F. J. G. Nanohole Plasmons in Optically Thin Gold Films. *J. Phys. Chem. C* **2007**, *111*, 1207–1212.
39. Hanarp, P.; Sutherland, D. S.; Gold, J.; Kasemo, B. Control of Nanoparticle Film Structure for Colloidal Lithography. *Colloids Surf., A* **2003**, *214*, 23–36.
40. Kanazawa, K. K.; Gordon, J. G. The Oscillating Frequency of a Quartz Resonator in Contact with a Liquid. *Anal. Chim. Acta* **1985**, *175*, 99–105.
41. Liedberg, B.; Lundstrom, I.; Stenberg, E. Principles of Biosensing With an Extended Coupling Matrix and Surface-Plasmon Resonance. *Sens. Actuators, B* **1993**, *11*, 63–72.